Advanced Composite Materials
Publication details, including instructions for authors and subscription information:
http://www.tandfonline.com/loi/tacm20

Real-time observation of damage nucleation in three-dimensionally reinforced carbon/carbon composites and role of bundle/matrix interface

Liming Wei [a], Songhe Meng [b], Chenghai Xu [b], Fei Qi [b] & Xiaoxiao Tian [b]

[a] Institute of Structural Mechanics, CAEP, Mianyang, 621900, China

[b] Center for Composite Materials, Harbin Institute of Technology, Harbin, 150080, China

Published online: 01 May 2013.

To cite this article: Liming Wei, Songhe Meng, Chenghai Xu, Fei Qi & Xiaoxiao Tian (2013) Real-time observation of damage nucleation in three-dimensionally reinforced carbon/carbon composites and role of bundle/matrix interface, Advanced Composite Materials, 22:3, 165-174, DOI: 10.1080/09243046.2013.791238

To link to this article: http://dx.doi.org/10.1080/09243046.2013.791238

Advanced Composite Materials, 2013
Vol. 22, No. 3, 165–174, http://dx.doi.org/10.1080/09243046.2013.791238

Real-time observation of damage nucleation in three-dimensionally reinforced carbon/carbon composites and role of bundle/matrix interface

Liming Wei[a]*, Songhe Meng[b], Chenghai Xu[b], Fei Qi[b] and Xiaoxiao Tian[b]

[a]*Institute of Structural Mechanics, CAEP, Mianyang 621900, China;* [b]*Center for Composite Materials, Harbin Institute of Technology, Harbin 150080, China*

(*Received 10 December 2010; accepted 27 March 2013*)

Carbon/carbon composites (C/Cs) are widely used as thermal protection materials in aviation and aerospace field. Most of the fracture processes of C/Cs have been found to be profoundly affected by their interfacial properties. Specially arranged fiber bundle push-out test was utilized to determine the fiber bundle/matrix interface shear strength of one three-dimensionally reinforced C/Cs. In order to reveal the link between the interfacial properties and the failure behavior, the micromechanisms of damage initiation at the notch tip on the C/Cs was investigated in real-time during the flexural fracture tests through scanning election microscopy. Real-time fracture observation revealed that the damage was nucleated in the fiber bundle/matrix interfaces around the notch tip and the failure crack was successfully observed along the fiber bundle/matrix interface. Fiber yarns acted as an obstacle to crack propagation hence it was necessary to increase the load to propagate the crack through the next fiber yarn.

Keywords: carbon/carbon composites; flexure fracture; fiber bundle; interfacial shear strength

1. Introduction

Carbon/carbon composites (C/Cs) consist of a fibrous carbon substrate in a carbonaceous matrix that display several advantageous properties for structural applications at high temperature up to 3000 °C in inert environments, along with low density, good strength retention at high temperature, high thermal and chemical stability in inert environments, and high thermal shock resistance. For this reason, applications of C/Cs in high temperature environments have been explored, especially in the aerospace fields, such as rocket nozzles, reentry vehicles' nosetips, and supersonic aircraft brakes.[1–4] However, when C/Cs is used, various disadvantages must still be overcome. These deficits include vulnerability to oxidation, poor matrix mechanical properties, and low interlaminar shear strength. To overcome the latter problems, three-dimensionally reinforced (3D-C/Cs) have frequently been introduced. In contrast to laminated (2D) C/Cs, 3D-C/Cs exhibit several superior mechanical responses, e.g. higher fracture toughness and strain capability.

Many investigators have expended an amount of effort toward the clarification of the mechanical behavior of C/Cs, especially from the viewpoint of fracture mechanisms.[5–11] Among numerous microfracture processes and mechanisms of C/Cs, the following

*Corresponding author. Email: hitwlm@yahoo.cn, hitwlm@aliyun.com

microscopic processes are by far the most important; namely, the first matrix cracking, crack-face fiber bridging, and the subsequent fiber pull-out from the matrix. Most of the fracture processes of C/Cs have been found to be profoundly affected by their fiber bundle/matrix interfacial properties. These results suggest that the characterization of the fiber bundle interfacial properties is necessary for understanding the unique mechanical behavior of 3D-C/Cs. Therefore, the precise evaluation of fiber bundle/matrix interfacial properties has become important. Several attempts have been made to measure the interfacial shear strength (IFSS) of C/Cs, for example, fiber push-in, push-out, and pull-out tests.[12–15] However, the IFSS of C/Cs has not been successfully determined, especially for the 3D-C/Cs.

In this work, IFSS of one 3D multidirectional textiled C/Cs were examined. The 3D multidirectional textiled C/Cs is referred to as T-3D-C/Cs. Specially arranged fiber bundle push-out tests were conducted for specimens with different thickness. The influence of thickness on the fiber bundle IFSS was also evaluated. Special attention is paid to the relationship between fracture mechanisms and the role played by the weak IFSS. Failure process of T-3D-C/Cs was investigated in real-time during the flexural fracture tests through scanning election microscopy (SEM).

2. Materials

The principal schemes of the bundle preform and optical micrograph of T-3D-C/Cs are shown in Figure 1. The preform of T-3D-C/Cs is made of dry carbon fibers and rigid carbon rods. Carbon rods are pultruded from 6000 high-strength carbon fibers T300 impregnated with unsaturated polyester resin. The rods inserted into the corresponding holes of upper and lower plates are aligned in square (Figure 1(a)). Carbon rods provide the *z*-direction reinforcement. The spacing between *z*-directional rod of T-3D-C/Cs forms channels in four directions. The *x*- and *y*-direction fiber bundles with different numbers were woven around straight *z*-fiber bundles. Two more ±45°direction fiber bundles with same numbers were placed in the *x*–*y* plane to give a five-directional reinforcement. Fiber bundles in the *x*-, *y*- and *z*-direction have different sizes and shapes. As can be seen in Figure 1(b), the cross-sections of bundles in the *z*-direction are nearly circular and their mean diameter is 1.5 ± 0.05 mm. Many relatively large pores are presented in the T-3D-C/Cs ranging in size from 30 to 50 μm. Most of them are located in the carbon matrix. The majority of these cavities appear to be closed, but some of them are interconnected or linked with cracks along the bundle/matrix interface.

The composite matrix was created in the course of carbon vapor infiltration and impregnating coal tar pitch. The product was subjected to a final graphitization treatment under high temperature about 2500 °C in inert atmosphere. According to our measurements, the density of T-3D-C/Cs is 1.87 ± 0.02 g/cm^3, which is 17% smaller than the ideal graphite density. A large part of this difference is due to different kinds of porosities. The fiber volume fraction of T-3D-C/Cs is about 47% and the porosity is about 7%.

3. Fiber bundle/matrix interface of T-3D-C/Cs

3.1. Interfacial shear strength

Several attempts have been made to measure the fiber/matrix IFSS of C/Cs using methods often adopted for other composites, including fiber push-in, push-out, and pull-out tests. However, to date, the IFSS of C/Cs has been successfully determined only by fiber push-out tests. [13,16] In this work, the fiber bundle push-out test was performed using an electric-driven testing machine at a displacement rate of 0.5 mm/min. The procedure of this test is illustrated

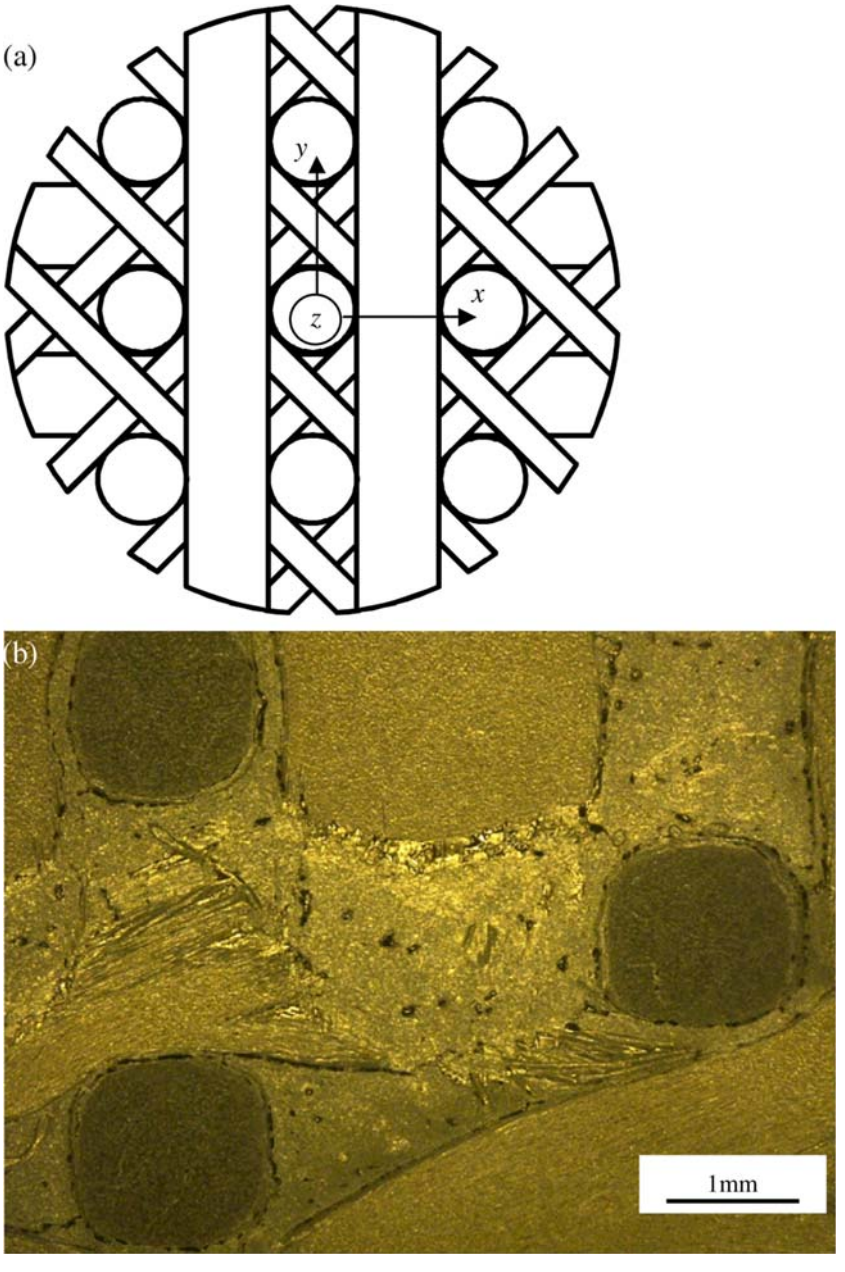

Figure 1. (a) Principal scheme of the preform with a Cartesian coordinate system for T-3D-C/Cs [3] and (b) T-3D-C/Cs as seen in the direction close to the *z*-direction.

in Figure 2. A 2 mm groove was drilled through the base plate so as to enable a fiber bundle to be pushed-out. Compressive load was directly applied to the specimen ends, the *z*-direction bundle of T-3D-C/Cs was extruded into the groove using a tungsten-carbide needle (diameter is 1.2 mm). The displacement was obtained from crosshead movements. The specimens were prepared by polishing a piece of T-3D-C/Cs first, and then finished into the needed thickness.

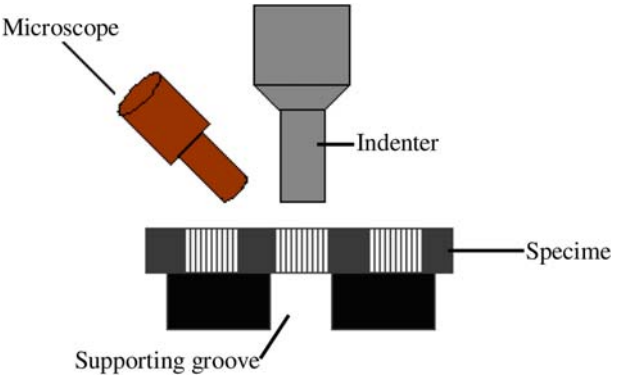

Figure 2. Schematic drawing of the fiber bundle push-out test fixture.

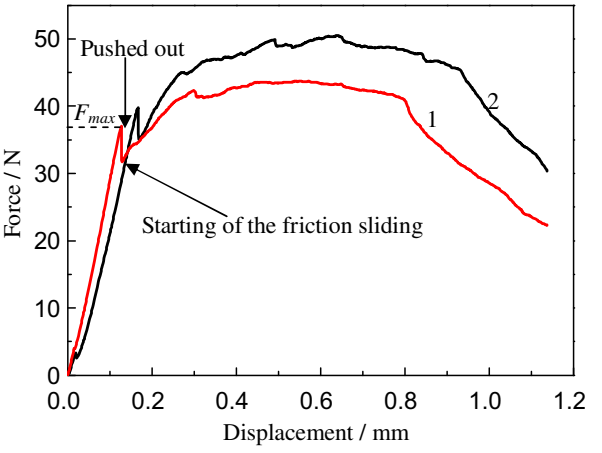

Figure 3. Typical relation between force and indenter displacement obtained by fiber bundle push-out test.

Figure 3 shows the typical load–displacement (L–d) curves for the z-direction fiber bundle push-out tests of T-3D-C/Cs. As can be seen in Figure 3, the fiber bundle push-out processes can be clearly divided into three stages. In the first stage, load rapidly increased up to the maximum value F_{max} and the rising curve was almost linear. Above F_{max}, an abrupt stress drop generally occurred in the L–d curve. This means that the test entered the second stage. It shows the fiber bundle sliding in this stage. The load abrupt increased and maintained after little change in displacement, this shows that the test had reached the third stage. This behavior can be resulted from the diamond indenter that came into contact with the surrounding matrix when the z-direction fiber bundle produced axial displacement.

In order to confirm the fiber bundle debonding and sliding, the fracture specimen surface of T-3D-C/Cs was observed via laser confocal scanning microscope (LSM). When the load surpassed the maximum value, a pushed-out z-direction fiber bundle without damage to the surrounding matrix was clearly observed as shown in Figure 4(a). It is evident that a shear fracture was successfully induced at the loaded z-direction fiber bundle/matrix interface.

Figure 4(b) is the typical three-dimensionally reconstructed image picture of a fracture specimen. Through this, the failure characteristic of z-direction fiber bundle/matrix interface

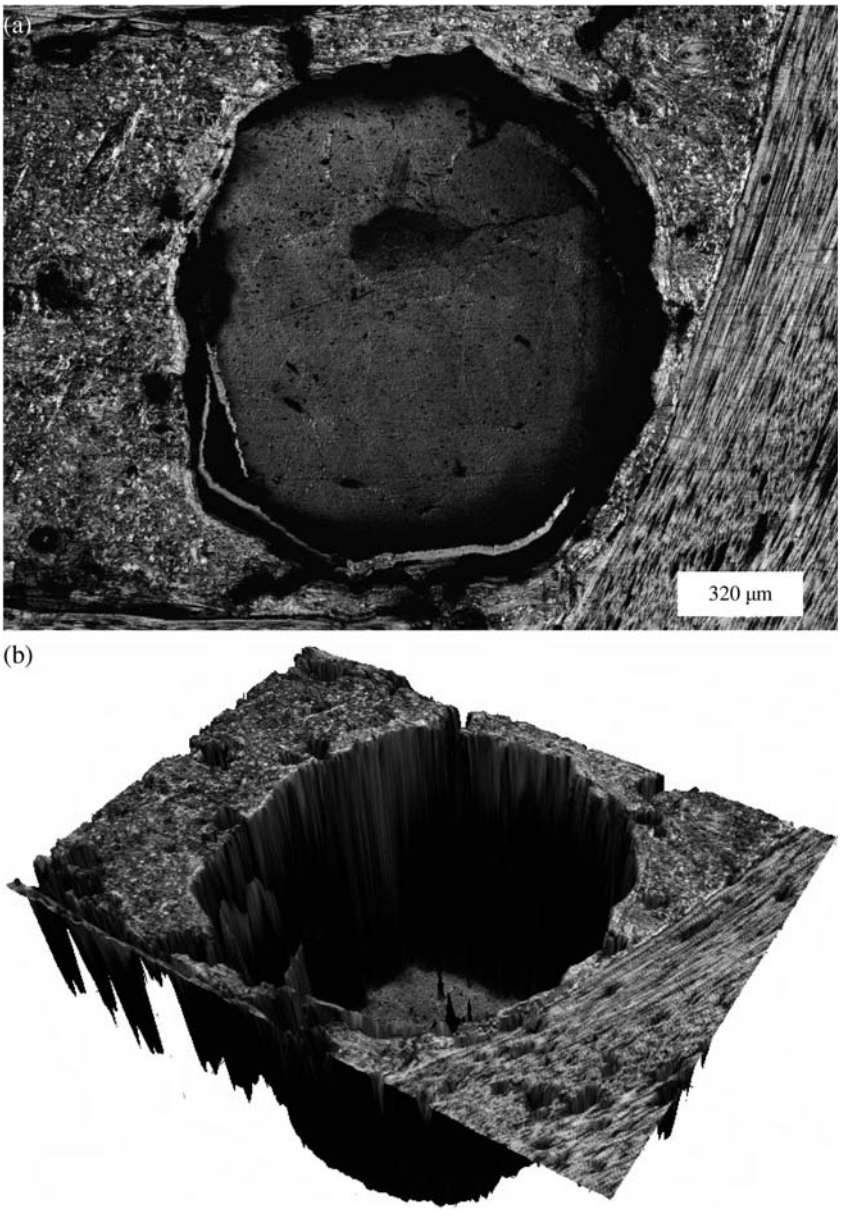

Figure 4. Images of T-3D-C/Cs specimen surface after push-out test. (a) LSM micrograph and (b) three-dimensionally reconstructed image.

in the push-out test will be able to make more clear observation. As observed in this picture, the *z*-direction fiber bundle was still moving along the inherent gap at the interface and little matrix block fragments are embedded to the surfaces of the loaded *z*-direction fiber bundle.

3.2. Effect of specimen thickness on IFSS

Under the assumption that the shear stress is uniformly distributed along the interface, the average approximated IFSS is given by the following Equation.

$$\tau = \frac{F}{2\pi R_f L} \quad (1)$$

where F is the load applied to a fiber when the interfacial debonding or sliding occurred, R_f is the fiber bundle radius, and L is the specimen thickness.

For the fiber bundle push-out test, the thickness of the specimen is an important factor affecting the test results. The stress distribution at interface will be affected by the thickness of the specimen. Many investigators have studied the relationship between the thickness and the IFSS, but their results were not consistent.[17–20] *Z*-direction fiber bundle specimens of T-3D-C/Cs with different thickness were chosen to be pushed-out for comparison in this work. Based on the Equation. (1), the average push-out forces and average IFSS values were listed in Table 1.

Table 1. Influence of specimen thickness on *z*-direction bundle push-out test results.

Thickness L (mm)	1.46	2.00	2.30	2.70
Push-out force F (N)	31.83, 34.83	39.50, 36.45	43.80, 37.17	49.33, 53.81
	27.13, 20.07	33.87, 34.25	37.42, 37.22	53.57, 58.37
	30.51, 19.93	43.50, 44.28	34.80, 41.30	67.89, 56.96
	34.13, 24.59	38.15, 43.42	35.91, 38.61	49.49, 60.71
	24.49, 31.77	29.76, 36.26	39.61, 38.46	57.12, 48.16
	23.66, 23.25	42.02, 43.36	37.44, 44.59	56.82, 46.65
	24.82, 25.89	38.64, 35.69	38.34, 38.14	47.34, 44.80
	27.59, 30.29	36.84, 39.89	39.14, 39.48	46.11, 47.74
	22.70, 25.87	47.52, 45.01	38.03, 37.60	57.07, 49.30
	22.94, 24.21	29.37, 44.31	39.50, 33.59	51.04, 48.80
	24.27, 25.87	46.07, 30.19	38.41, 40.47	50.90, 54.50
	19.96		42.62, 46.72	64.80
			35.76, 33.69	
			36.41, 38.79	
			33.82, 44.58	
Average force $\bar{F}$ (N)	25.84	39.02	38.71	53.10
Dispersion coefficient	16.67%	13.59%	8.29%	11.24%
Average IFSS $\bar{\tau}$ (MPa)	3.89	4.28	3.69	4.32

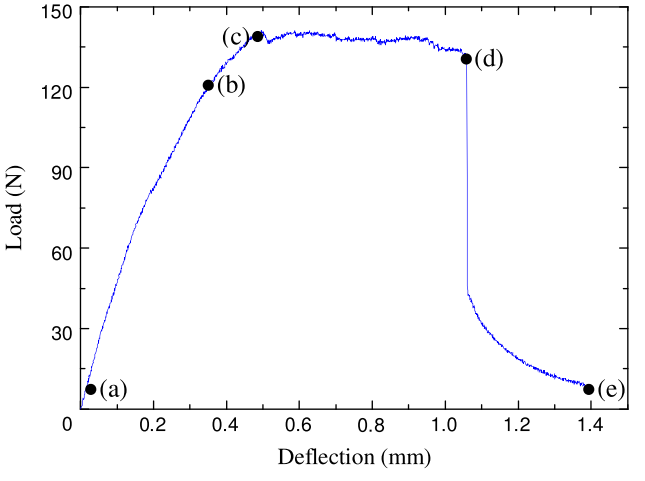

Figure 5. Typical loading–deflection curve for *z*-direction notched specimen of T-3D-C/Cs.

The data in Table 1 showed that the *z*-direction IFSS value of T-3D-C/Cs is relatively small;, they have no IFSS value more than 5 MPa. Such low IFSS value would significantly affect the failure behavior of T-3D-C/Cs. As can also be seen in Table 1, the IFSS value gradually increases as the specimen thickness increases. However, IFSS of specimen with $L = 2.3$ mm is different from increasing tendency. The values of dispersion coefficient of specimen with $L = 2.3$ mm is far below than those of others. So, $L = 2.3$ mm can be used as the standard thickness of the *z*-direction fiber bundle push-out test of T-3D-C/Cs in later experiments.

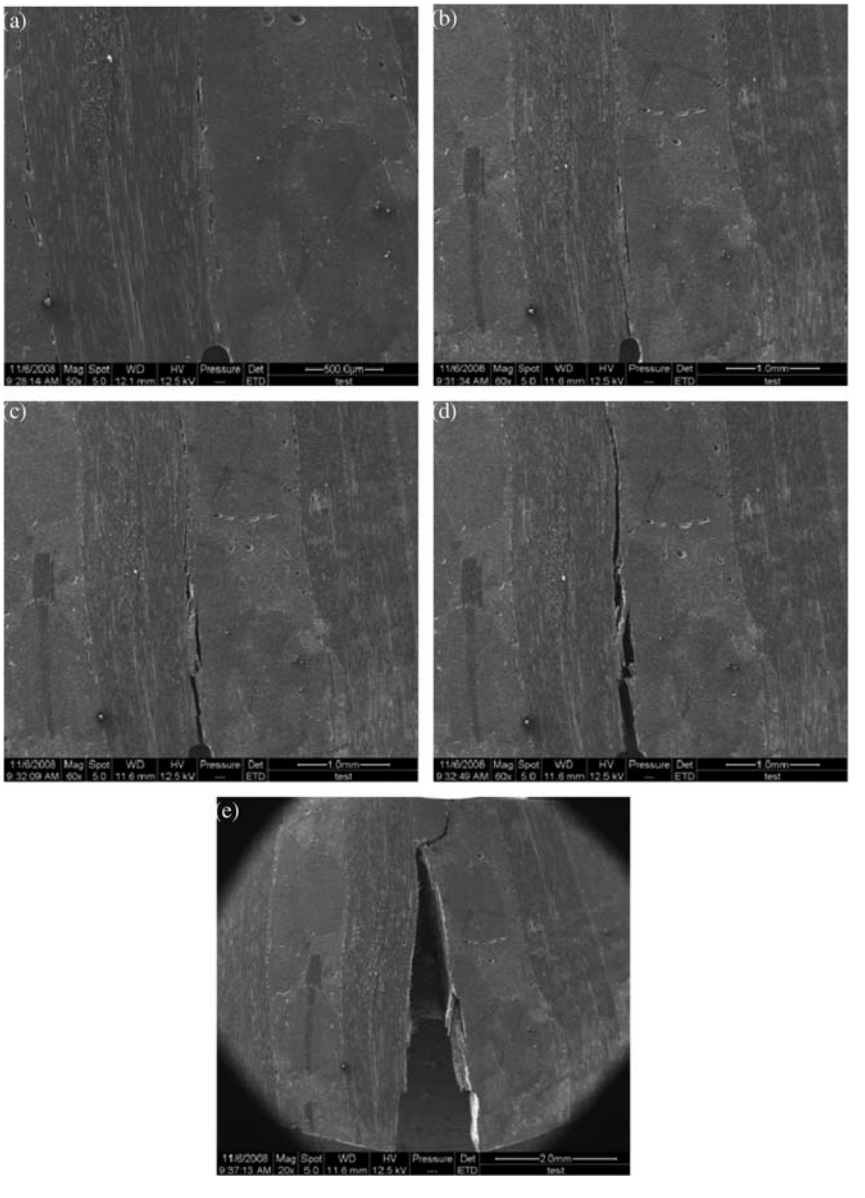

Figure 6. Development of damage around the notch tip for *z*-direction flexural specimen at (a) the beginning of the test; (b) 80% of the maximum load; (c) maximum load; (d) the end of load stabilization and (e) the final failure specimen. The precise load for each micrograph is given in Figure 5.

4. Damage nucleation of T-3D-C/Cs

Direct observation of crack nucleation for C/Cs can provide a more direct link between the fracture process and the bundle/matrix interface. And, it can be used to determine the features of crack initiation in the C/Cs specimen. The macromechanical test of T-3D-C/Cs was performed in servo-mechanical testing machine using a three-point bend fixture. The fixture was placed in a SEM device. The flexural test in the T-3D-C/Cs was preformed with the flat specimen. The flat specimen has 6 mm height, 35 mm span, and the thickness is 3 mm. The finite notch tip radius of *z*-direction flexural specimen is approximately 100 μm. The cross-head displacement rate of flexural test was 0.5 mm/min.

The load–deflection curve of T-3D-C/Cs for the *z*-direction flexural specimen is plotted in Figure 5 and the corresponding damage initiation micromechanisms are shown in the micrographs (Figure 6(a)–(e)) which were taken, respectively, at the beginning of the test, at the 80% of the maximum load, at maximum load, at the end of load stabilization, and when the load had dropped by approximately 95%. As can be seen in Figure 5, the initial response of the composite was linear. As shown in Figure 6(a), the notch tip was located in the fiber bundle/matrix interface. According to the structure of T-3D–C/Cs (Figure 1(a)), most of the load was be carried by *z*-direction fiber bundles when the specimen was undergoing bend load. As the load increased, the notch tip propagated along the fiber bundle/matrix interface. The only damage detected in the *z*-direction flexural specimen of T-3D-C/Cs prior to the failure was a crack of approximately 1.5 mm in length, which grew from the notch root (Figure 6(b)). No cracks perpendicular to the notch axis were found, this shows that the crack had directly crossed through the *z*-direction fiber bundle. As also can be seen in Figure 5, the load maintained a long-time stabilization after the peak load point. After this, the load rapidly decreased. This indicated that the *z*-direction fiber bundles had been broken completely.

The fracture photograph of *z*-direction bending specimen of T-3D-C/Cs was shown in Figure 7. This figure showed that the pulled-out fibers failure character was observed in the lower half part of the *z*-direction bundle and a completely brittle facture occurred in the upper

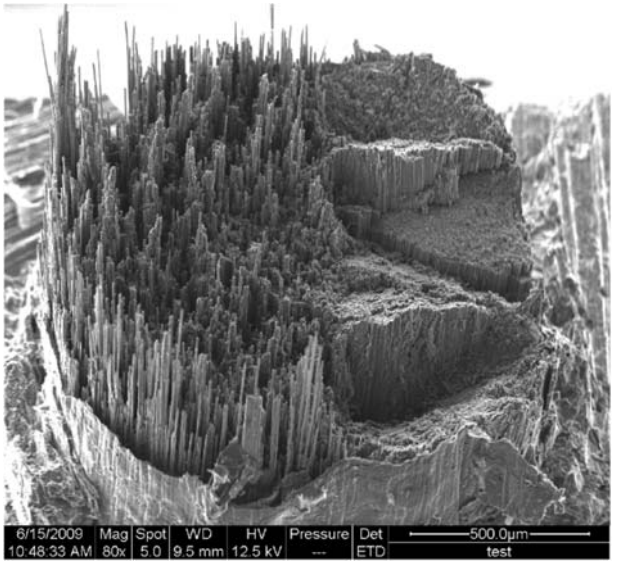

Figure 7. Fracture surface of the *z*-direction flexure specimen.

half part of *z*-direction bundle where specimen bears compressive load. The fibers tensile pulled-out failure process corresponds to the stage from (c) to (d) in Figure 5. As can also be seen in Figure 7, a section of *z*-direction bundle was pulled out and the bundle/matrix interface was undamaged. It showed that the weak bundle/matrix interface obviously influenced the fracture character of the *z*-direction flexural specimen.

5. Conclusions

The author has presented an experimental analysis of fiber bundle/matrix interface properties of T-3D-C/Cs. The *z*-direction fiber bundle IFSS was successfully obtained by the push-out test methods. The IFSS increased monotonically with the specimen thickness. The real-time observation of damage nucleation showed that the *z*-directional flexural specimens seem to be sensitive to the pre-notch. The damage was nucleated in the fiber bundle/matrix interfaces around the notch tip and the forces could be better transmitted in the specimen. Fiber yarns acted as an obstacle to crack propagation and it was necessary to increase the load to propagate the crack through the next fiber yarn.

Acknowledgments

This work was performed within the research program of the National Science Foundation of China under the grant #11202198. The authors are also indebted to Dr H. B. Shi for providing the materials. The following acknowledgment is made research sponsored by the New Century Educational Talents Plan managed by the Chinese Education Ministry under construct #NCET–06–0338.

References

[1] Park SJ, Lee JR. Bending fracture and acoustic emission studies on carbon-carbon composites: effect of sizing treatment on carbon fibres. J. Mater. Sci. 1998;33:647–651.
[2] Fitzer E, Manocha LM. Carbon reinforcements and carbon/carbon composites. Berlin: Springer; 1998.
[3] Buckley JD, Edie DD. Carbon-carbon materials and composites. New Jersey: Noyes Publications; 1992. P12.
[4] Han JC, He XD, Du SY. Oxidation and ablation of 3D carbon-carbon composite at up to 3000 °C. Carbon. 1995;33:473–478.
[5] Sakai M, Miyajima T. Fiber bridging of a carbon fiber-reinforced carbon matrix lamina composite. J. Mater. Res. 1991;6:539–547.
[6] Sakai M, Miyajima T. Matrix cracking and fiber bridging of a carbon fiber reinforced carbon matrix composite. Fract. Mech. Ceram. 1992;9:69–82.
[7] Suzuki T, Sakai M. Fiber pullout processes and mechanisms of a carbon fiber reinforced silicon nitride ceramic composite. J. Mater. Res. 1992;7:2869–2875.
[8] Cao JW, Sakai M. The crack-face fiber bridging of brittle matrix composites. Fract. Mech. Ceram. 1996;11:163–176.
[9] Leon M Jr. Micromechanical modeling of strength and damage of fiber reinforced composites. PhD thesis: Technical University of Denmark; 2007.
[10] Aly-Hassan MS, Hatta H, Wakayama S, Watanabe M, Miyagawa K. Comparison of 2D and 3D carbon/carbon composites with respect to damage and fracture resistance. Carbon. 2003;41: 1069–1078.
[11] Hatta H, Taniguchi K, Kogo Y. Compressive strength of three dimensionally reinforced carbon/carbon composite. Carbon. 2005;43:351–358.
[12] Sakai M, Matsuyama R, Miyajima T. The pull-out and failure of a fiber bundle in a carbon fiber reinforced carbon matrix composite. Carbon. 2000;38:2123–2131.
[13] Furukawa Y, Hatta H, Kogo Y. Interfacial shear strength of C/C composites. Carbon. 2003;41:1819–1826.
[14] Chandra N, Ghonem H. Interfacial mechanics of push-out tests: theory and experiments. Compos. Part A. 2001;32:575–584.

[15] Li M, Matsuyama R, Sakai M. Interlaminar shear strength of C/ C-composites: the dependence on test methods. Carbon. 1999;37:1749–1757.
[16] Aoki T, Ogasawara T, Ishikawa T. Shear behavior and fiber bundle interfacial properties of 3D-C/ C composites, in: Proceedings of the 8th international SAMPE JPN Tokyo; 2003. p. 845–848.
[17] Yang CJ, Jeng SM, Yang JM. Interfacial properties measurement for SiC fiber-reinforced titanium alloy composites. Scr. Met. Mater. 1990;24:469–474.
[18] Yang JM, Jeng SM, Yang CJ. Fracture mechanisms of fiber-reinforeced titanium alloy matrix composites, Part 1: interfacial behavior. Mater. Sci. Eng. 1991;A138:155–167.
[19] Netravali AN, Stone D, Ruoff S, Topoleski ITT. Continuous microindenter push-through technique for measuring interfacial shear strength of fiber composites. Compos. Sci. Tech. 1989;34:289–303.
[20] Roman L, Aharonov R. Mechanical interrogation of interfaces in monofilament model composites of continuous SiC fiber-aluminum matrix. Acta. Metal. Mater. 1992;40:477–485.